Thesis for the degree

Master of Science

Submitted to the Scientific Council of the

Weizmann Institute of Science

Rehovot, Israel

עבודת גמר (תזה) לתואר

מוסמך למדעים

מוגשת למועצה המדעית של

מכון ויצמן למדע

רחובות, ישראל

By

Idan Hochner

מאת

עידן הוכנר

The Molecular Beam Machine: A Cold Molecular Ion Generator

מקור ליונים מולקולרים קרים באמצעות קרן מולקולרית

Advisor:

Ziv Meir

מנחה:

זיו מאיר

Febuary 2023

פברואר תשפ"ג

Abstract

Trapping atomic ions using Paul traps is a leading method in many fields at the forefront of research. Recently, methods of sympathetically cooling molecular ions in Paul traps using quantum logic have been developed, which enable trapping and cooling them to gain quantum and coherent control. This promises exciting avenues of research, including new types of quantum superpositions, studies of many-body physics, molecular metrology, and many others.

We aim to build a Paul trap for trapping molecular ions, this thesis presents the first part of this journey, building a molecular-ion source. We have built a machine that generates molecular beams using supersonic expansion and optimized the ionization of molecules to a specific rotational state using state-selective resonance-enhanced multi-photon ionization (REMPI). For this, we have integrated into the machine a homemade time-of-flight mass spectrometer with a resolution high enough to resolve masses of at least 250 amu for REMPI optimization.

We demonstrated the ionization scheme on N_2, a relevant molecule for quantum coherent control, showing its REMPI spectrum and finding its ionization threshold at 125666 cm^{-1}. The generality in which the machine is operated makes this a reliable and diverse source for optimizing and generating molecular ions for future experiments.

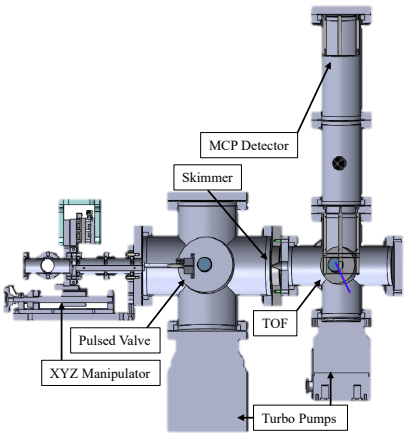

The molecular beam machine used to optimize the molecule ionization.

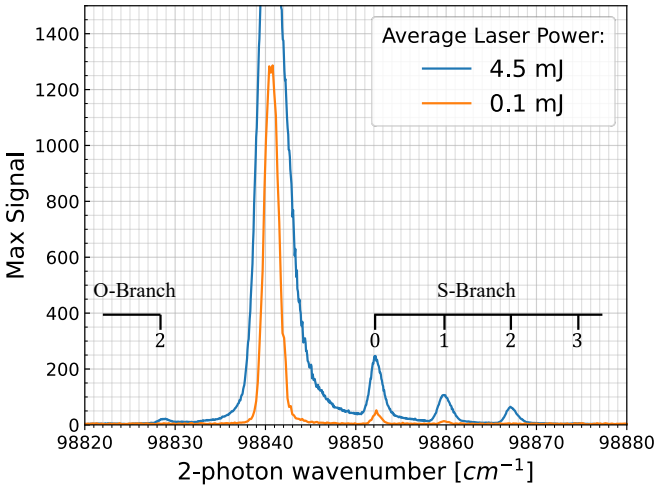

The single-color REMPI spectrum of N_2.

Acknowledgments

Experimental work, especially physics-related experiments, is rarely done alone. This project, which was built from scratch, owes much of its success to the Department of Physics of Complex Systems workshop employees. I would especially like to mention Guy, for his help in the design of the home-built parts. His experience and work integrity are priceless, often guiding me away from making mistakes, allowing me to use the workshop when it was needed, and always finishing the designs and the parts ahead of time.

And of course I would like to thank my advisor, Ziv Meir, none of this would have been achieved without his guidance and help. Thanks for your patience in teaching me the scientific and technical work in the lab. For the support and helping hand when doing things for the first time or the hundredth time. And I especially thank you for accepting me early on and trusting me with this project which began even before the official start of your position. It has been a diverse and challenging experience, leaving me with a big appetite to continue this experiment.

מֵהַכֹּל נִשְׁאֲרוּ רַק שְׁלוֹשָׁה דְּבָרִים:
הַיְדִיעָה שֶׁאֲנַחְנוּ תָּמִיד בַּהַתְחָלָה
הַיְדִיעָה שֶׁאֲנַחְנוּ חַיָּבִים לְהַמְשִׁיךְ
הַיְדִיעָה שֶׁיַּפְסִיקוּ אוֹתָנוּ לִפְנֵי
הַסִּיּוּם.
לַעֲשׂוֹת מֵהַהַפְסָקָה דֶּרֶךְ חֲדָשָׁה
לַעֲשׂוֹת מֵהַנְּפִילָה צַעַד שֶׁל מָחוֹל
מֵהַפַּחַד - גֶּשֶׁר
וּמֵהַחִפּוּשׂ - מִפְגָּשׁ

פרננדו פסואה

List of Abbreviations

APV Amsterdam Piezo Valve

FL Flash lamps

$FWHM$ Full width at half maximum

I_2 Molecular iodine

m/z Mass to charge ratio

MCP Multi-channel plate

MS Mass spectrometer

N_2 Molecular nitrogen

N_2^+ Ionized molecular nitrogen

PC Pockel's cell

$REMPI$ Resonance enhanced multi-photon ionization

SHG Second harmonic generator

std Standard deviation

THG Third harmonic generator

TOF Time of flight

UHV Ultra-high vacuum

Contents

1 Introduction

Quantum mechanics is one of the most fascinating scientific theories, as it introduces probability as an integral part of nature. It successfully explains the molecular and atomic structures compiling our universe and the formation of different phases of matter. The surprising outcomes of the postulates of quantum mechanics, such as interference and entanglement, have been thoroughly sought out and experimentally proven. With this firm knowledge, it is compelling to develop new and advanced methods and technologies which rely on the unique traits of quantum mechanics. These would demand very precise and coherent control of such a system.

Such quantum-mechanical control has been gained and demonstrated in systems of atoms and atomic ions [1, 2]. A famous application of this control is the development of optical clocks [3]. This broadened the field of precision measurements and has reignited the discussion over the definition of the basic unit of time [4]. Only in the last couple of decades began demonstrations of such control of molecules [5, 6] and molecular ions [7, 8, 9, 10]. Molecules are advantageous to atoms in their diversity and range of sizes and weights. They also hold unique characteristics due to their more complex structure. The field of quantum control of molecules holds many prospects, such as new types of quantum superpositions [11], studies of many-body physics, molecular metrology [12, 13], and many others. These make molecules attractive candidates for emerging quantum technologies.

To observe the quantum mechanical nature of a particle, it must be sufficiently isolated from the environment and its temperature sufficiently low. To control a particle in a quantum-mechanical manner, it will typically be confined in a trapping potential, of which are common the magneto-optical trap, the RF Paul trap and others. Using a Paul trap [14], atomic ions can be stored in the trap for days and even years, and can be manipulated with exceptionally high operation fidelity [15]. In a Paul trap, specific types of ions (alkaline-earth ions or similar) can be readily laser-cooled to their motional ground state [16]. Other ions, not suitable for laser cooling, can be co-trapped with a suitable ion and sympathetically cooled [17] to their ground state and detected using quantum logic [18] techniques. The majority of molecules are of the second type of ions; they cannot be laser cooled because they lack closed transitions due to their complex energy structure. The high fidelity, long storage time, and quantum logic make the Paul trap an ideal device for quantum control of molecules [19, 20].

Sympathetic cooling of a molecular ion co-trapped with a laser-cooled ion can cool the external degrees of freedom of the molecule, but not its internal degrees of freedom [21]. An internally cold molecular ion can either be generated using state-selective photoionization [22], buffer-gas cooling [23] or through chemically bonding a cold atom with a neutral [9]. In this thesis, we use the state-

selective photoionization approach.

Due to the challenges mentioned above, only a handful of groups worldwide study trapped molecules [24]. Considering the vast amount of molecules available, building a device to cool and manipulate molecular ions holds great promise for scientific and technological applications.

This thesis presents my work on designing and building a machine for generating internally-cold ionized molecular nitrogen (N_2^+). The state-selective ionization is optimized using a home-built time-of-flight (TOF) mass spectrometer (MS) integrated with the machine. The machine can be easily converted to generate other atomic or molecular ions and is designed to connect to a vacuum chamber holding a Paul trap.

I will present the final design of the machine and the spectroscopic results for the different steps in optimizing the state in which the molecular ions are generated. I will also present the rotational spectrum of the ionization process $N_2 \rightarrow N_2^+$ and the opening of the ionization channel of the rotational and vibrational ground state.

2 Goals

We aim to build a cold atom-molecule ion trap to study the quantum mechanics of molecules and to use the molecules' quantum mechanical properties for new experiments. The goal of this study was to create a cold molecular ion source. The method of cooling we chose relies on generating cold molecules using supersonic expansion and ionizing them to a low rotational and vibrational state using state-selective ionization. To optimize this molecular source, we designed and built a time-of-flight mass spectrometer with a mass resolution of 250 and more.

The main objective of this work has been to build an operable and optimizable molecular beam machine, that is ready to connect to an ion trap. We aimed to measure the different transitions of molecular nitrogen (N_2) and to optimize the setup for ground-state ionization. The machine was designed and built also to be able to optimize molecules heavier than N_2 (28 amu), specifically with molecular iodine in mind (I_2, 254 amu).

The molecule, N_2^+, has been proposed as a suitable candidate for creating new quantum superpositions [11], high precision spectroscopy, and tests of fundamental constants [25]. The molecule, I_2^+, is a promising candidate to probe dark matter through variations of fundamental constants [26]. Generating N_2^+ for ion trapping using this method has been demonstrated by several groups [27, 28]. Following these reasons, building a cold source of N_2^+ molecules is achievable, and will be a good vantage point for further experiments.

3 Methods

3.1 Supersonic Expansion

Most atomic ions are generated using an oven to vaporize the solid form of the atom. Generating molecules this way will heat up their rotational and vibrational states, and will require cooling those afterward. Instead, we choose to generate our molecular ions at cold internal states as possible. For this, we prefer using resonance-enhanced multi-photon ionization (REMPI) [27], a selective ionization technique, which will be described in detail in section 3.2. Selective ionization techniques require using specific transitions, the first being from the neutral's ground state. This means the process is most efficient when the molecular gas is sufficiently cold, and the ground-state population is maximal. To generate molecules with a well-defined energy distribution, we use a cold molecular beam generated by supersonic expansion through a pulsed valve [29, 30]. In supersonic expansion, high-pressurized gas is injected through a small nozzle ($\sim 100\ \mu$m) into a very low-pressure chamber (typically $< 10^{-5}$ mbar) and expands in a densely packed high-velocity distribution at very low temperatures (typically < 5 K) [31].

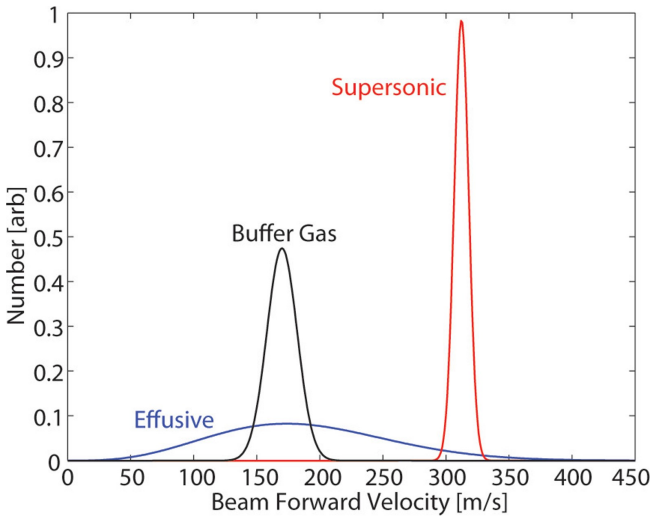

Figure 1: The velocity spread of different types of molecular beams. Taken from [31].

Molecular beams have been used in scientific experiments for over a century. It is a part of many prosperous scientific fields such as molecular collision studies and chemical reaction studies [32]. Advances in pumping technologies, laser technology, and detection methods make this tool relevant and popular still today. Nozzle shapes are fabricated to give the beam density an optimal expansion [33], also, pulsed gas sources enable generating beams from higher pressures while maintaining ultra-high vacuum (UHV) conditions. These output in colder and denser molecular beams.

3.2 Resonance-Enhanced Multi-Photon Ionization (REMPI)

Multiple methods of control of molecular ions require the preparation of the molecule's internal states, REMPI is a selective photoionization method to do that. This method has become popular due to the abundance of spectroscopic data available for many atomic and molecular species and the growing range of pulsed laser sources.

As its name hints, several photons are absorbed in all REMPI processes for the neutral to be ionized. Usually, photons of one wavelength will be absorbed to excite the neutral to an intermediate state. Then, another photon of the same wavelength, or another wavelength, is absorbed and ionizes the neutral [34]. The selectivity of the REMPI process comes from the fact that molecular spectroscopy is directly involved in the ionization process. The simplest REMPI will use two photons of the same wavelength, while other processes, using more photons and more wavelengths, can be developed to infinite complexity. The closer the wavelength of the photons is to the transition wavelength in the neutral, the higher the transition probability. Added to this is the photon absorption probability that decreases approximately to the power of the number of photon absorptions involved. On top of that, the transition selection rules and the states' overlap dictate the possibility and lifetime of the transition. Upon these rules, the system's neutral density and the available photon flux will ultimately determine the feasibility of the REMPI process.

Selective REMPI processes that ionize molecules to a specific rotational and vibrational state can serve as a first step for quantum-state preparation, ground-state cooling of the external motion, and coherent manipulation of molecular quantum states. Several of these processes were developed for N_2^+ for this exact purpose. N_2^+ is particularly interesting for experiments in quantum control because of its symmetric structure and low reactivity.

Mackenzie et al. have shown a 2+1' process (presented in figure 2a), which generates N_2^+ by exciting it to an intermediate Rydberg state using two photons of 202 nm and ionizing it from this intermediate state to the ground state of the ionized molecule using one 375 nm photon [35]. I will continue denoting transitions using a second wavelength using a prime and the ones using the first wavelength, or only one wavelength, without it. A downside to this method is that 2+1 ionization using only 202 nm photons is also possible through an above-threshold ionization, which generally is not state selective. Since the first transition wavelength is more energetic than the second, the contribution of this non-selective process is significant. Gardner et al. devised a different 2+1' REMPI scheme (presented in figure 2b) exciting through an intermediate transition at 255 nm and ionizing to the ground state with a 212 nm transition [27]. Since 2+1 ionization in this scheme isn't energetically

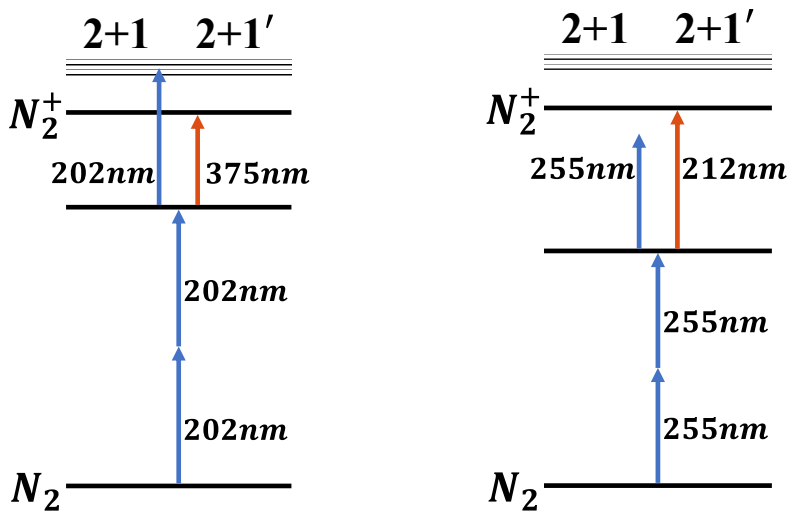

(a) Mackenzie et al. [35] **(b)** Gardner et al. [27]

Figure 2: N_2 REMPI methods. (a) $X^1\Sigma_g^+\,(\nu=0) \rightarrow a''^1\Sigma_g^+\,(\nu=0) \rightarrow X^2\Sigma_g^+\,(\nu=0)$. (b) $X^1\Sigma_g^+\,(\nu=0) \rightarrow a^1\Pi_g\,(\nu=6) \rightarrow X^2\Sigma_g^+\,(\nu=0)$.

feasible, better state selectivity is expected. Our system supports both schemes, but we decided to begin with the first (less state selective) scheme due to its stronger spectroscopic signal.

3.3 Time-Of-Flight Mass Spectrometry (TOF-MS)

Initially, MS was invented by J. J. Thompson about a century ago to measure the mass-to-charge ratio (m/z) of the electron [36]. Having successfully accomplished this, MS took a vital part in the discovery of isotopes of different elements. Today MS is extremely popular in the field of chemical analysis, where many types of spectrometers were invented, and is one of the primary tools used in all scientific disciplines. TOF-MS was first used in 1946 [37], and it was further improved by Wiley and McLaren in the following decade [38]. In the last few decades, as detection and computing speeds grew faster, TOF-MS has become more popular due to its versatility and simplicity.

There are two basic principles in TOF-MS. The first, particles with different m/z ratios, will accelerate differently in static electric fields [39]. The second, particles with the same m/z but with different initial positions and momenta, that are accelerated by an electric field, will focus in time on a specific plane perpendicular to the accelerating field. This plane is where a detector is placed.

The first principle emerges from the basic kinematics of a charged mass in an electric field. Let's assume a charged mass at rest, with mass m and charge z, is accelerated a distance a in an electric field E_a (in V/cm). The particle's electric potential is $U_a = aE_a$. The time it takes the mass to pass

this distance is:

$$t_a = \sqrt{\frac{2ma}{zE_a}},$$

and the velocity of the mass after acceleration is:

$$v_f = \sqrt{\frac{2zU_a}{m}}.$$

Thus, the time it will take the mass to traverse a distance, D, following the acceleration will be:

$$t_D = D \cdot v_f^{-1} = D \cdot \sqrt{\frac{m}{z} \cdot \frac{1}{2U_a}},$$

and the total time is a function of $\sqrt{m/z}$.

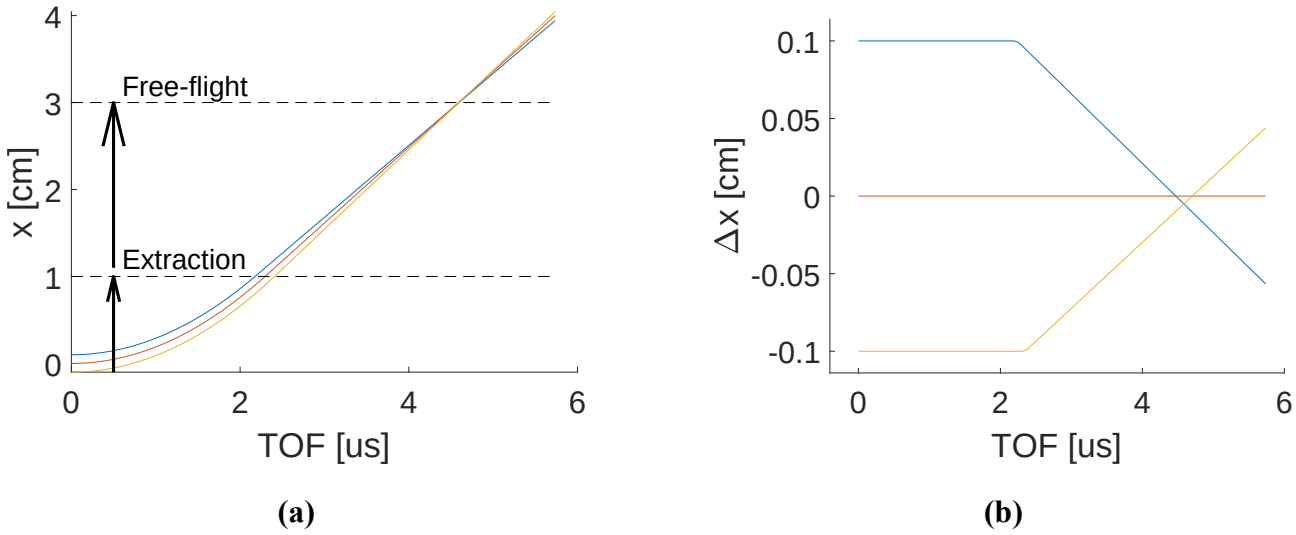

(a) **(b)**

Figure 3: Example of ion focusing in time. (a) Calculated trajectory of ions with different initial positions accelerated to an extraction electrode, then continued in free flight. The dashed line marked "Free-flight" marks the distance where the ions arrive with the smallest time difference. (b) The distance of the ions from the ion starting at position $x = 0$ as function of the TOF time.

The second principle emerges if we variate the initial position by exchanging $a \to a + \delta$, and look for D that gives the minimal change in the total TOF:

$$\frac{d(t_a + t_D)}{d\delta} = 0.$$

A charge with a positive δ will have a longer t_a, but will also gain a higher v_f, meaning that it will eventually "catch up" with a charge with a smaller or negative δ. Figure 3 shows these principles. The transition of the ions from a zone with an electric field to a zone with a weaker field (or without one at all) gives a focusing effect in time. In general, manipulating ions using static electric fields is called electro-static lensing.

Usually, electrodes with different potentials are used to generate electric fields. The two electrodes surrounding the region in which ions are formed (the extraction region) will be named “repelor” and “extractor” and are shown in figure 4. The first is the electrode the particles accelerate away from, and the second is the electrode the particles accelerate towards. Thus, U_a is the extraction voltage and varies with the initial position of the ion between the repelor and extractor. Using just these two electrodes, as in figure 3, the plane of focus is at a constant position around half the distance in which the particles are accelerated:

$$D = \frac{a}{2}.$$

In this constellation, the resolution of the TOF-MS is limited by the time-resolving abilities of the detector and the length of time ions are generated. Both should be shorter than the smallest TOF difference between two consecutive masses in the spectrum.

Following [39] and Wiley and McLaren’s design [38], we can add a third electrode, an ”accelerator”, in a plane following the extractor. Adding the accelerator, and increasing even more the particles’ energy, allows controlling the position of the plane of focus. This means another electric field, E_b, is added, accelerating the charge a distance of b. This changes the total electric potential to $U_{total} = U_a + U_b$. The distance where the TOF variation is minimal becomes $D(U_{total}/U_a)$. Increasing D will give a larger TOF, and larger TOF differences, which can overcome the limit set by the detector’s time resolution and the ion generation time.

For the rest of the discussion, we assume singly charged positive ions, meaning that $m/z = m$. This means that the TOF is linear in $\sqrt{m}$, and if we know the TOF of m_1, then the TOF of any other mass will be:

$$TOF_{m_2} = TOF_{m_1}\sqrt{\frac{m_2}{m_1}}. \tag{1}$$

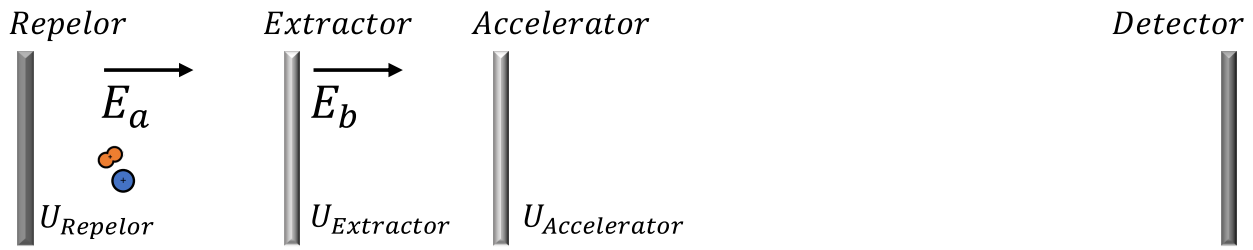

Figure 4: Diagram of the Wiley and McLaren TOF-MS [38]. Ions are created between the Repelor and the Extractor electrodes and are accelerated by a constant electric field, E_a. The total potential of the ions depends on their initial position between the Repelor and Extractor electrodes. Following the Extractor electrode, the ions are accelerated by a second constant electric field, E_b. Following the Accelerator electrode, the ions perform a field-free flight until they reach the detector.

3.4 Experimental Setup

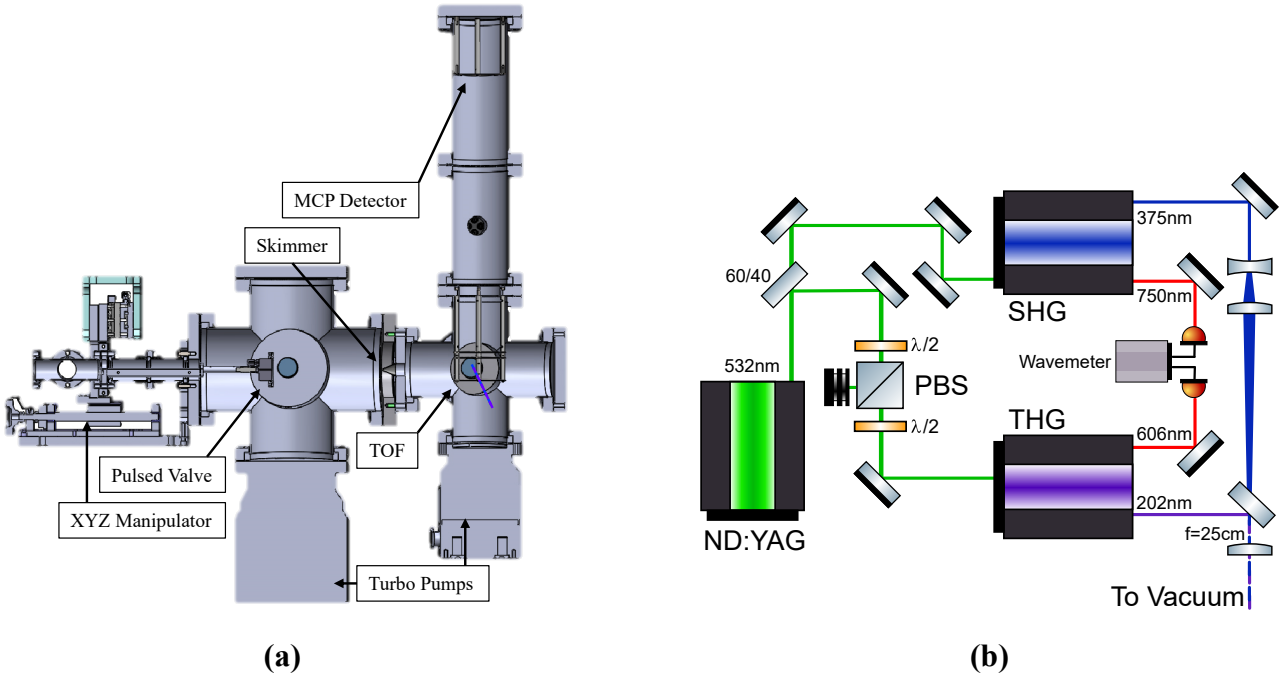

(a) **(b)**

Figure 5: (a) A cutaway of the experimental system. The blue and purple lines mark the ionization lasers. (b) Diagram of the optical setup.

3.4.1 Vacuum System

The vacuum system is designed to sustain molecular beam generation and is shown in figure 5a. The system is made of two stainless steel ultra-high vacuum chambers. The first chamber is pumped by an Edwards NEXT730D turbo-molecular pump to a background pressure under 10^{-8} mbar. This chamber contains an Amsterdam Piezo Valve (APV) mounted on a mechanical XYZ stage that can

be controlled from outside the chamber. The second chamber is pumped by an Edwards nEXT300T turbo-molecular pump to a background pressure of around 10^{-8} mbar. This chamber contains a home-built TOF-MS, its electrodes are centered around the molecular beam path, and its acceleration and free-flight regions are perpendicular to the beam path. Both chambers are separated by a skimmer from Beam Dynamics (Model 2, 2mm orifice) that collimates the molecular beam to the TOF chamber and keeps the chamber pressure from rising even when the APV is being operated. Both pumps are backed by an Edwards nXDS15i scroll pump. Gauges are located in each chamber and between the scroll pump and the turbo-molecular pumps, and the pressure is monitored continuously using Grafana [40], a peek of the Grafana interface is shown in figure 6.

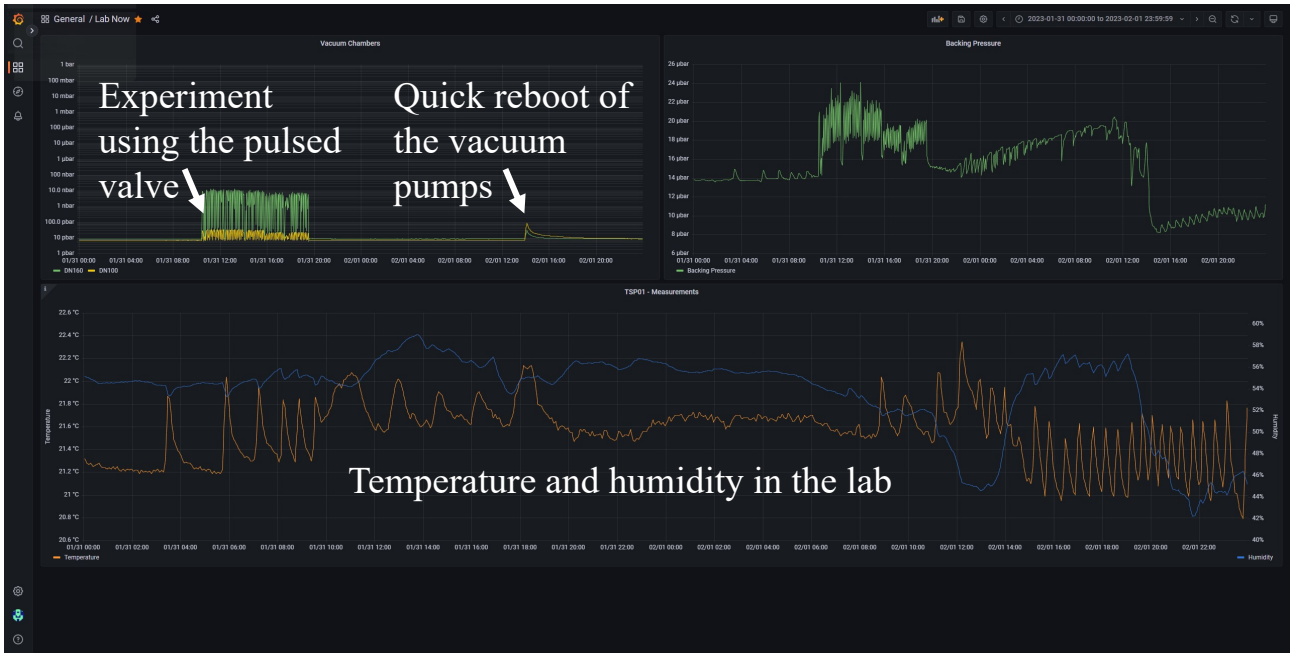

Figure 6: An exemplary screenshot of the Grafana interface showing the pressure measurements of the vacuum chambers and backing pressure and the temperature and humidity in the lab.

3.4.2 Laser Setup

We ionize our nitrogen molecular beam using a 2+1' REMPI scheme. Both REMPI colors are generated by dye lasers pumped by the second harmonic of a pulsed Nd:YAG laser (532 nm, Innolas SpitLight) generating 5 ns pulses at a rate of 10 Hz. The excitation stage is done by the third harmonic generation (THG) of a dye laser (Lioptec, Liopstar) producing 202 nm light (3:1, Rhodamine 6G:DCM, in ethanol). The ionization stage, is done by the second harmonic generation (SHG) of a second dye laser (Lioptec, Liopstar) producing 375 nm light (Styryl 8, in ethanol). A diagram of the optical path of the laser setup is illustrated in figure 5b. The output energies of the pulsed lasers were

typically between 100 μJ to 5 mJ, and the wavelengths were measured and monitored using a High Finesse WS6 wavemeter with an accuracy of 0.01 cm^{-1}. Between the pump and the THG we placed a polarizer and a polarizing beam splitter to allow us to lower the relative output energy of the THG compared to the output energy of the SHG.

Both lasers are focused by the same lens (f=250mm) into the center of the second vacuum chamber. The 375 nm beam passes through a telescope that expands it and focuses it slightly into the lens to compensate for the beam's longer focal distance. The telescope is made from a scattering lens and a focusing lens to avoid focusing the beam tightly outside the vacuum chamber and ionizing the air. The beams were overlapped through a 202 nm mirror back polished, allowing transmission of the 375 nm beam through it.

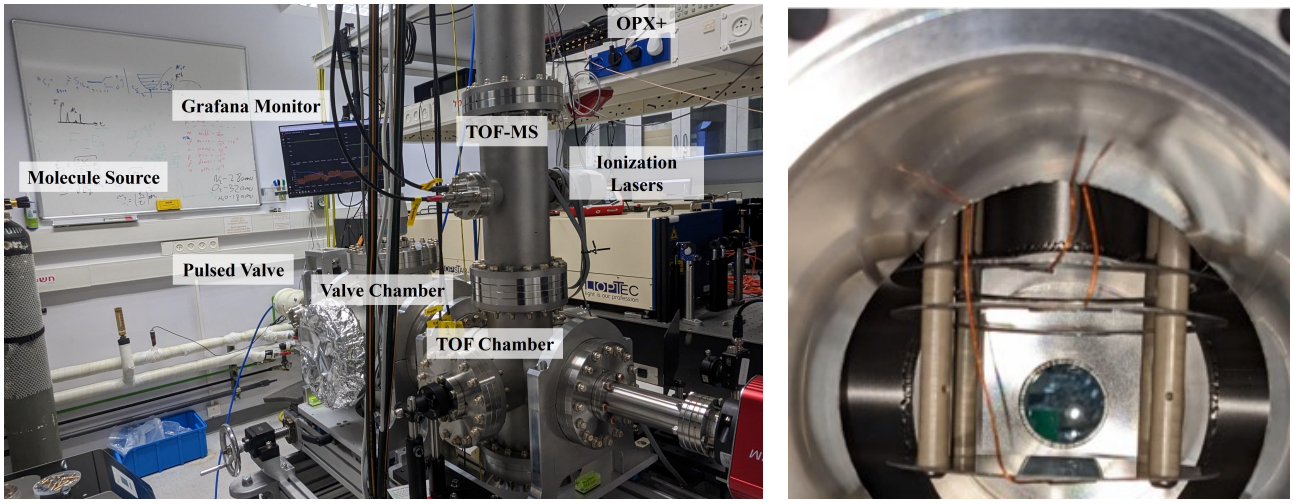

(a) **(b)**

Figure 7: Pictures of the setup. (a) The whole setup. (b) The TOF electrodes inside the vacuum chamber.

3.4.3 Time-of-Flight Mass Spectrometer

The generated ions are measured by a TOF-MS located in the second vacuum chamber, a photograph of the chamber is in figure 7b. The TOF-MS is a two-stage Wiley-McLaren, perpendicular to the molecular beam's propagation axis. It was designed based on simulations using SIMION [41], a more detailed review of these simulations is in 4.1. The TOF electrodes are positioned so that the lasers are precisely focused in the plane between the repelling electrode and the extracting electrode. The distance between these two electrodes is 4 cm, making the ion extraction length 2 cm. This also means that the ions gain in the extraction stage:

$$E_k = \frac{1}{2}\Delta V_{Extraction}\, eV$$

$$\Delta V_{Extraction} = V_{Repelor} - V_{Extractor}$$

The second stage is a 1 cm acceleration region, and the accelerator electrode is set to ground. The extractor and accelerator are nickel mesh grids with 95% open area transmission spot-welded to stainless steel rings. The final stage is a 51 cm drift region. Ions extracted by the TOF-MS are accelerated to a multi-channel-plate (MCP) detector (Photonis, chevron MCP 40-12-10-8 D 46:1) with a ground-cathode, voltage on the MCP can be tuned to 2kV, and the voltage on the metal anode is 2.5kV.

A detailed photograph of the whole setup inside the lab is shown in figure 7a.

3.4.4 Control Hardware

The APV, pump laser, and MCP detection window, are triggered by Quantum Machines' OPX+, an easily programmable control hardware for "synchronized multi-channel pulse sequences, pulse parametrization, real-time classical calculations, complex flow control with real-time decision making, and ultra-low latency feedback" [42]. With the OPX+, the delay between triggers can be easily changed with a 1 ns resolution, and the output signal can be directly measured. It can also easily synchronize using simple python scripts other devices such as wavemeters, power meters, shutters, and more.

The OPX+ and the rest of the instruments in the experimental setup can be controlled using Python scripts. All of the output data is saved in CSV files.

A typical experiment pulse sequence is shown in figure 8, other triggered sources can be easily added to any of the ten outputs of the OPX+. The reason that after triggering the pump laser's flash lamps (FL) the OPX+ is being triggered back by the Pockel's cell (PC) trigger is in order to lower the actual laser output's time uncertainty. When the pump laser's FL are triggered, there is an error of 3 ns for the output beam, to reduce this error to 1 ns, we use the trigger the pump laser outputs when it pulses the PC to release the laser beam. Except for MS, all other experiments are performed by operating the typical pulse sequence and observing the TOF ion signal, while in between sequences a parameter is changed.

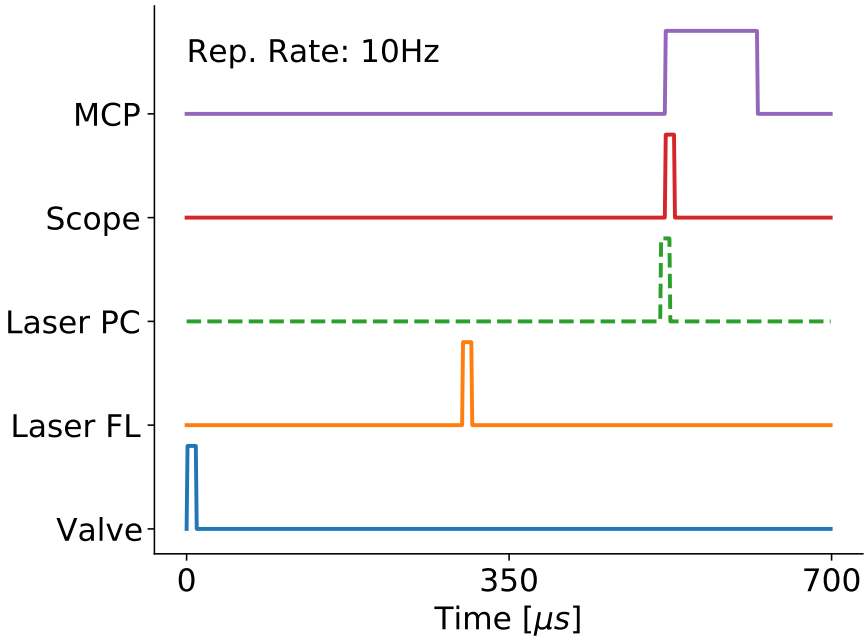

Figure 8: A typical TOF pulse sequence generated by the OPX+. FL stands for the pump laser's flash lamps, which start the lasing. PC stands for Pockels cell, which releases the pump laser's beam and outputs a trigger voltage. The dashed line indicates this pulse is an input trigger generated by the pump laser and it triggers the OPX+ to continue. The MCP pulse width indicates the measurement window and is exaggerated in this figure.

4 Results

4.1 Simulating a TOF-MS Using SIMION

The goal of this project was to build a versatile machine, that can efficiently work with the light N_2 which has an atomic mass of 28 amu, and the heavier I_2 which has an atomic mass of 254 amu. The TOF-MS is the final piece of this "puzzle" and is thus constrained by the methods mentioned above. The parts the TOF-MS will be constructed from, need to be of reasonable size and length for the workshop to build. The voltages set on the electrodes need to be able to be generated by a common power supply. The use of a supersonic expansion beam means ions generated will have a supersonic initial velocity in the beam direction. Using REMPI means ions will not be generated instantaneously but during the whole duration of the laser's 5-ns pulse. This means that masses arriving at the detector within a window of 5 ns will not be distinguishable. Lastly, the total TOF is proportional to $\sqrt{m}$, and the difference in the TOF of two consecutive masses will shorten as their mass grows.

Thus, our TOF-MS will be limited in distinguishing between masses by the short TOF difference of the heavier masses in the system, meaning that resolving I_2 will be more difficult than resolving N_2. To meet the above constraints, we performed numerical calculations of the TOF-MS using the software

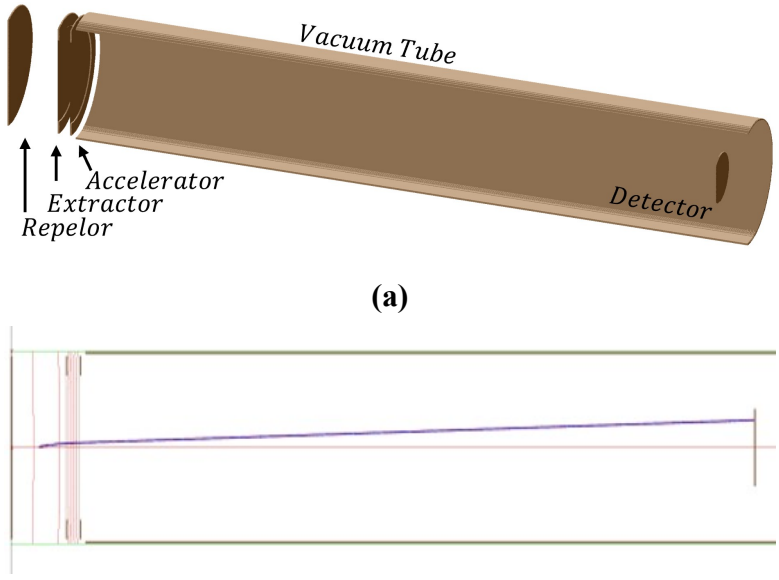

Figure 9: The Simion environment. (a) 3D model of the generated electrode configuration of the TOF design. (b) Picture of the SIMION software GUI of a simulation of random particle trajectories in the generated model. Electrodes are marked in brown, and particle trajectories in blue. The horizontal red line is the TOF axis, and the vertical red lines are the electric-equal-potential lines.

SIMION 8.1 [41]. These simulations validated the design works with the mentioned constraints and helped find the optimal dimensions and electrode voltages for operation.

For the actual design, I followed the basic design of Wiley and McLaren [38], and chose the simple three-electrode TOF setup like in figure 4. In this setup, the accelerator is grounded, and the voltage on the repelor and extractor is positive. Referring to the sizes introduced in section 3.3, if we assume to ionize the molecules exactly in between the two electrodes, then:

$$U_a = \frac{U_{Repelor} - U_{Extractor}}{2},$$

$$U_{total} = U_{Extractor} + U_a.$$

When realizing such a system, all sizes become finite and regions of free flight in a vacuum are bound by the vacuum chamber. These boundary conditions make the electrostatic problem difficult to solve. The SIMION software simplifies solving this problem. In the SIMION software's environment, one can design a 3D configuration of electrodes, set the voltage of each electrode, and generate different particles to see their trajectory. The software simulates the electric fields using the finite-difference method to solve Laplace's equation and calculates particle trajectories using the Runga-Kutta method and dynamically adjusted time steps. Initial conditions can easily be changed, and random particle position and velocity distributions can be easily generated.

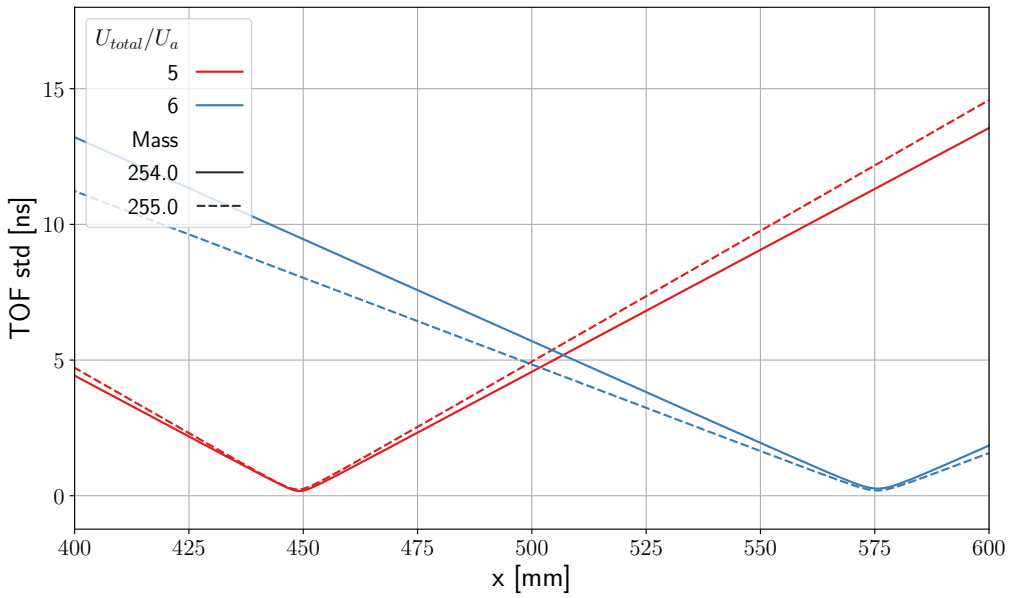

Figure 10: The std of the TOF of 40 ions as a function of the distance for different masses and at different voltage ratios. The minimum point of each line is the plane of focus of the ions.

Using the software, I created an environment of electrodes identical to the actual TOF-MS design in our vacuum system (Figure 9). To approximate the length of the free-flight region which will give the system a sufficient mass resolution, I ran multiple simulations with random ion distributions, varying the voltage ratio in each simulation, and looking for the distance where the TOF standard deviation (std) was minimal. Figure 10 shows how the std changes during a trajectory, minimizing at about the same distance for different masses. At the minimal distance, the std is well under 5 ns, the length of the laser pulse, meaning the TOF uncertainty will be completely dictated by the laser. The figure also shows how that the distance grows with the voltage ratio.

The actual distance of the plane was determined by the length of the catalog vacuum tubes, and a tube was chosen to be in a distance giving a TOF difference larger than 10 ns between two consecutive masses, at least twice the uncertainty due to the laser pulse. Figure 10 shows that between 500 mm and 600 mm will do. After determining the distance to place the detector, I simulated the TOF at this distance for smaller increments of the voltage ratio.

The change in the TOF spectrum of a slight shift of the voltage ratio is shown using two simulations in figure 11. In these simulations, random distributions of masses of 254 amu and 255 amu were generated around the center between the repelor and extractor; Their TOF was measured at the detector and the TOF mean and std were extracted to determine the resolution. To find the optimal voltage ratio, we maximize the TOF-MS resolution [39], which can be obtained using multiple definitions:

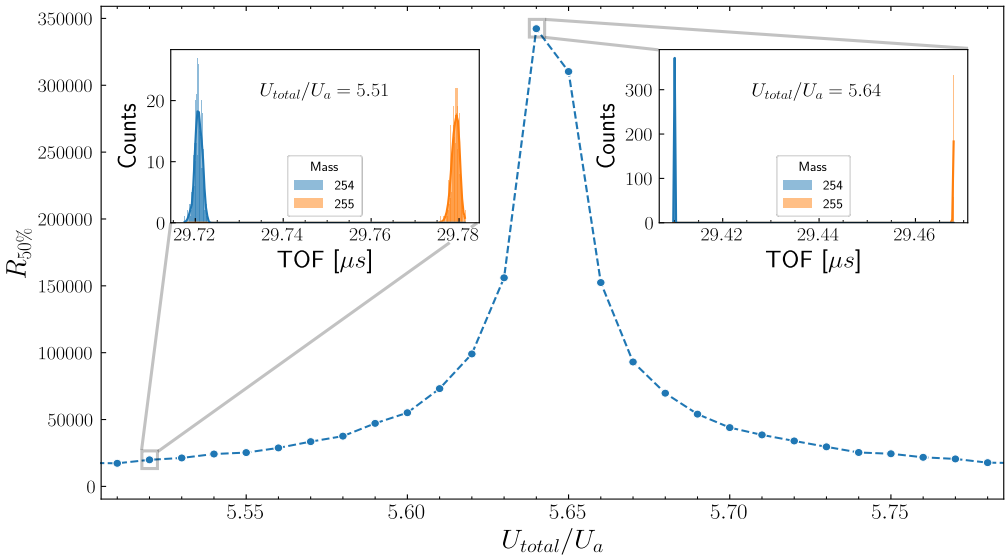

Figure 11: The resolution (Eq. 2) as a function of the voltage ratio. For each point the resolution was extracted from the histograms of the TOF. The insets zoom in on two of these points emphasizing how the peak width changes between the two. Each simulation generated 400 ions of each mass.

$$R_{50\%} = \frac{m}{\Delta m} = m\frac{TOF_{m+1} - TOF_m}{std(TOF_m)} = \frac{TOF_m}{2std(TOF_m)}. \tag{2}$$

Figure 11 shows the TOF-MS resolution, calculated using the TOF difference of two consecutive masses and the TOF std, as a function of the voltage ratio. The figure shows that for I_2 and its neighboring masses, the TOF difference is ~50 ns. At a voltage ratio of 5.64, the width of the TOF peak of I_2 and its neighboring masses narrow to beneath 0.1 ns, giving $R_{50\%} \approx 350,000$.

4.2 TOF Spectrum

We tuned the 202 nm laser to the exact wavelength of a very strong transition of N_2 (the Q transition, which will be discussed in 4.4), and looked at the arrival times of ions to our TOF-MS detector. We observed a strong peak at 7150 ns which we assigned to N_2^+ molecules. We validated this by observing a decrease in the signal when we moved the laser wavelength away from resonance with N_2, and an increase in the signal when we opened the pulsed valve (delivering more N_2 molecules into the vacuum chamber). An example of TOF measurements is shown in figure 12 when the APV is open (orange) and when it is closed (blue). The difference between the two measurements is also shown in green.

Two peaks appear in the data when the APV is on, the rightmost is the peak of N_2 that was validated.

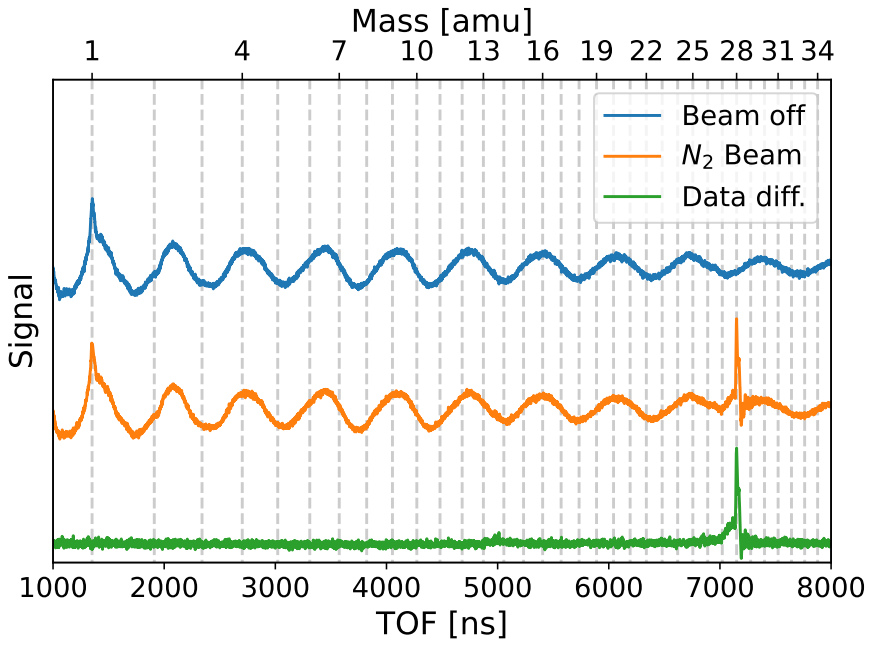

Figure 12: Average over 20 consecutive TOF traces when the APV is open (orange) and closed (blue) taken in an interlaced manner. The difference between both plots is shown in green. The mass axis is drawn with respect to the peak of N_2 at 7150 ns.

The mass of the ions creating the leftmost peak can be found using equation 1:

$$m = \left(\frac{TOF_m}{TOF_{N_2}}\right)^2 m_{N_2} = 0.998\ amu.$$

According to this analysis, we assign the peak to H^+ ions.

H^+ appears in our TOF-MS signal probably due to its dissociation from organic molecules residing in the vacuum chamber. Using this method, we can easily approximate the TOF of other singly charged ions (see upper axis in figure 12). When subtracting the measurement when the APV is off from the measurement with it on, the H^+ peak disappears, suggesting that our molecular-beam is pure. In addition, a small peak appears to be around the expected peak of m=14 amu. This makes sense as we use strong laser pulses, ions of N^+ are likely to form as well, and possibly some N_2^{+2} ions. As our main ionization method uses multiple photons, ionizing other molecules with different masses is difficult without tuning our lasers beforehand to a resonant wavelength of those molecules.

We can estimate our TOF-MS mass resolution using equation 2, by looking at the difference signal of the N_2^+ peak at full width at half maximum (FWHM). The TOF peak of N_2^+ is shown in figure 13, the peak is at $TOF_{28} = 7150$ ns and its $FWHM_{28} = 31$ ns. The mass-resolution of our TOF-MS system is thus $R_{50\%} \approx 100$, meaning that we can determine the masses we can distinguish using:

$$\Delta m = \frac{m}{R_{50\%}}.$$

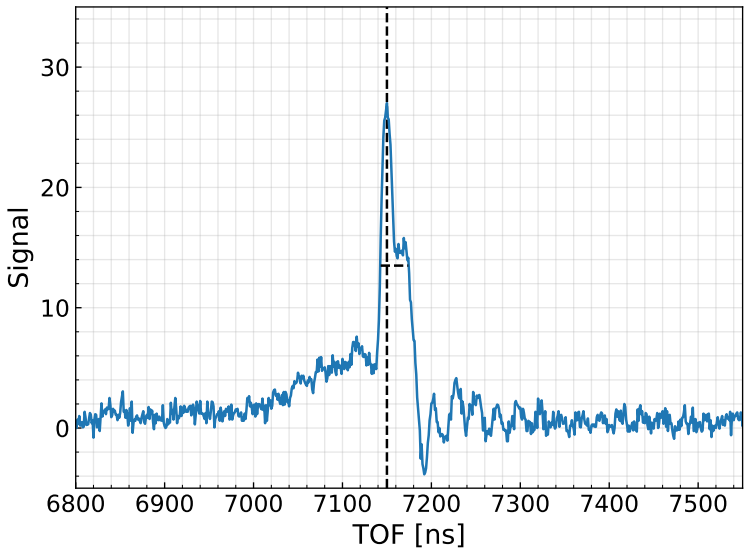

Figure 13: Zoom in on the peak of N_2^+ from the data difference in figure 12. The mean and FWHM are marked with dotted black lines.

For N_2^+, $\Delta m \approx 0.2$ amu, allowing to easily distinguish between molecules that differ from N_2^+ by a single mass unit. For I_2^+, $\Delta m \approx 2.5$ amu, higher than a single mass unit. However, this resolution should be sufficient for optimizing I_2^+ ionization, because molecules and atoms of its neighboring masses are rare and are not expected to show up in the TOF spectrum.

We got a resolution much smaller than the maximum in the simulation. The main reason for this is that the measured TOF peak is much broader than the simulated one. The 5 ns width of the laser pulse is one reason for this broadening. Figure 13 also shows that the measured peak is not continuous but has two parts and causes strong oscillations in the signal, this means that to truly calculate the TOF peak we need to reduce the noise and ringing of our measurement circuit.

4.3 Overlapping molecular beam and lasers

Here, we characterize the molecular-beam profile as a function of the pulsed-valve open time. We focus on the N_2^+ peak in the TOF spectrum, which is proportional to the number of N_2 molecules overlapping the ionization laser, and look at the change in peak height. To find the molecular-beam width, we change the time delay between opening the pulsed valve and triggering the laser (see figure 14). We repeat the experiment for different valve-open time values. Instead of a symmetric Gaussian-like molecular-beam profile, we observe a double-peak distribution. We suspect that the second peak is an artifact of the valve's shutter bouncing open in the process of closing itself.

From the maximum of the pulse profile, we can deduce the valve-laser delay, ~ 535 μs, for inter-

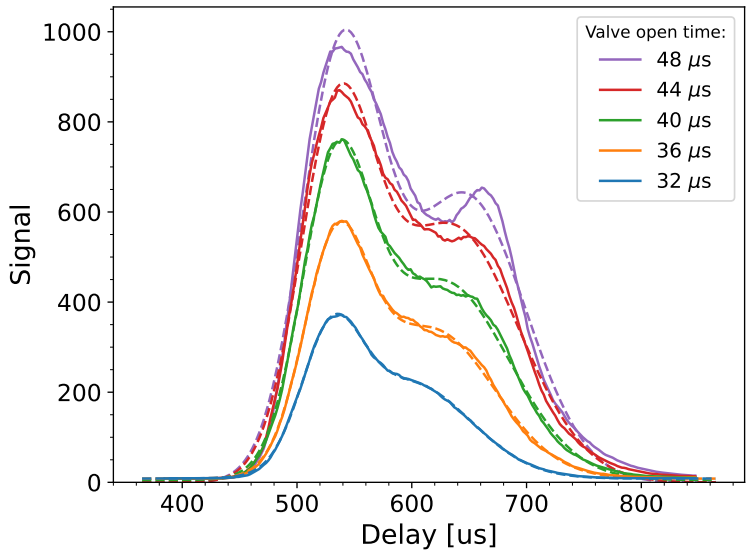

Figure 14: Molecular-beam temporal profile for different valve-open times. The signal is proportional to the number of N_2 molecules ionized by the laser's pulse and was smoothed using a 20 us moving average. The x-axis is the valve-laser delay. The dashed lines are double-Gaussian fits used to calculate the FWHM of the first peak. The black dashed lines show each individual Gaussian found in the fit for the measurement at a valve open time of 32 μs.

acting with the peak density of the molecular beam. This value is independent of the valve-open time value. We use double-Gaussian fits in figure 14 to separately characterize the two peaks in the pulse profile. The first peak corresponds to a faster and narrower pulse, with an average FWHM of $\sim$70 μs. The second peak corresponds to a slower and wider pulse, with an average FWHM of $\sim$130 μs. By dividing the distance of the valve from the ionization region (38 cm) by the peak density delay time, we can deduce the velocity of the beam to be 710 m/s. The spatial width of the beam is the velocity of the beam multiplied by the temporal FWHM, which gets broader by a few mm as the valve-open time is increased, this width increases from 9 cm to 13 cm.

To obtain the best spatial overlap between the lasers and the molecular beam, we scanned the laser's vertical position while monitoring the REMPI signal. We also checked that both lasers participating in the 2+1' REMPI scheme temporally overlap. This was done using a photodiode (ThorLabs, DET10A2) placed in the beam path right before the viewport of the TOF-MS vacuum chamber. Each dye laser pulse was measured over 600 shots while the other was covered. The resulting overlap is shown in figure 15, the mean is plotted using a filled line and the edges show the measurement std. The THG has a mean arrival time of 6.9 ns and a pulse width of 5 ns, and the SHG has a mean arrival time of 8.2 ns and a pulse width of 6 ns. The 2 ns delay between the two laser pulses can be compensated for using a delay line.

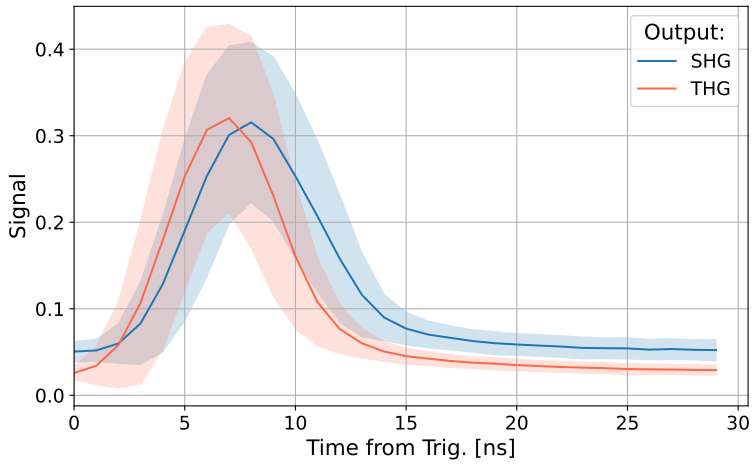

Figure 15: Temporal overlap of the two lasers participating in the 2+1' REMPI scheme. The x-axis is the delay between the PC trigger sent by the pump laser and each dye laser's laser beam reaching the vacuum chamber.

4.4 Nitrogen REMPI Spectrum

The "REMPI spectrum" of N_2 is the spectrum of transitions between the electronic-ground and electronic-intermediate states of neutral N_2 that participate in the REMPI process. We record this spectrum by performing 2+1 REMPI while scanning the 202 nm laser's exact wavenumber (the 375 nm laser is blocked). Figure 16 depicts the scan results for both high and low laser powers. Our results fit well with the results of [35].

The largest peak in the spectrum corresponds to the Q(J) transitions, in which the electron transitions from a low electronic state to a higher electronic state without changing its rotational state $(\Delta J = 0)$. The left-most peak corresponds to the O(2) transition, in which the electron transitions from the second rotational state at the lower electronic state to the ground rotational state at the higher electronic state $(J' = 0 \leftarrow J'' = 2)$. The right peaks correspond to the S-branch transitions, in which the electron's final rotational state is higher by two from the initial rotational state $(\Delta J = +2)$.

The rotational-state resolved O and S branches are of importance since from these transitions we know the initial and final rotational states of the molecule. This is opposed to the Q(J) transitions which are not rotational-state resolved by our laser's linewidth. Among these selective transitions, the S(0) transition is the most dominant and will be the transition we pass through when adding the 375 nm laser in the 2+1' REMPI scheme. For the low-power setting of ~ 0.1 mJ/pulse we were still able to resolve the S(0) peak and also record the non-saturated peak of the Q(J) transitions.

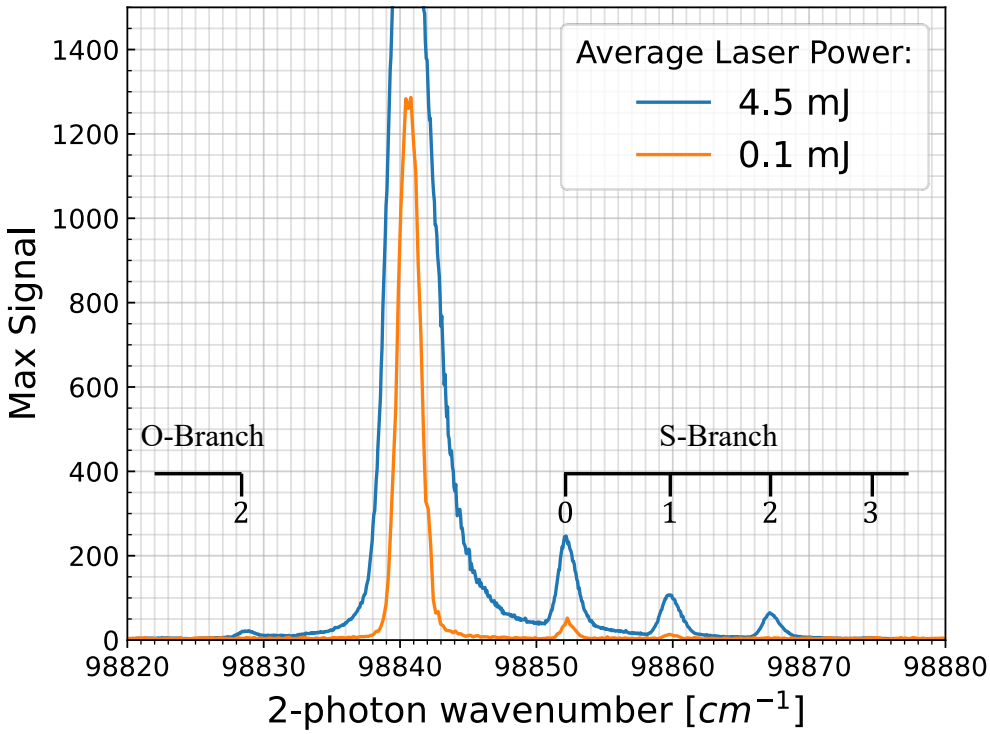

Figure 16: The single-color REMPI spectrum of N_2. The wavelength was scanned both forward and backward, at increments of 0.2 cm^{-1} and each point was averaged over 20 shots.

4.5 Nitrogen threshold-ionization spectrum

In the 2+1' REMPI scheme, the second photon is tuned close to the ionization threshold such that energy conservation adds an additional restriction to the possible final states of the ionized molecule. Here, we tune the 202 nm laser on-resonance with the S(0) transition and scan the 375 nm laser below and above the ionization threshold. We monitor the intensity of the N_2 TOF peak, which is proportional to the number of ionized molecules, as a function of the 375 nm laser's wavenumber, looking for a step-like increase in the signal intensity when passing the ionization threshold. This increase is due to the REMPI ionization method, the second transition in the molecule moves the electron from one Rydberg state to a higher Rydberg state, which is part of a series of states converging to N_2^+. When the energy becomes high enough, an ionization channel opens.

In figure 17a, we compare 2+1' and 2+1 REMPI signals. We scan 100 term values (the energy of the molecule from its ground-state) and repeat the experiment 50 times for each term value. We notice the 2+1' signal starts at a low steady-state value, then increases at the term value of 125610 cm^{-1} until reaching a higher steady state 50% larger at the term value of 125620 cm^{-1}. The 2+1 signal, as expected, is constant throughout the measurement (we raise the term values scanning the 375 nm laser, which doesn't participate in the 2+1 REMPI scheme). It is interesting to note that the

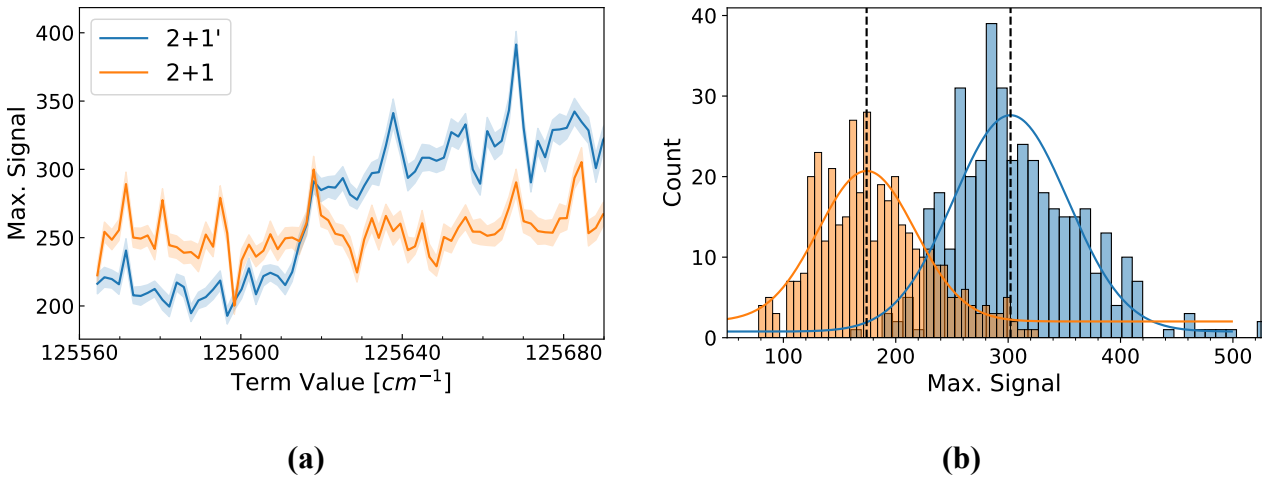

Figure 17: 2+1' REMPI signal. (a) An example of the spectrum of the 2+1' (blue) and 2+1 (orange) signals (in the 2+1 the scanned laser is blocked). The bold lines are the mean of the measurements, and the edges indicate the standard error. (b) Histogram of the same data in (a) for the data point with term value of 125650 cm^{-1}.

2+1' signal is lower than the 2+1 signal below 125615 cm^{-1}. This means that below the threshold, the 375 nm light inhibits ionization by the 202 nm light [43].

The term value of the N_2^+ electronic vibrational and rotational ground state is ~125666 cm^{-1} [35]. In figure 17a, we see that the 2+1' ionization starts at a lower value of ~125610 cm^{-1}. This is most likely due to the reduction of the ionization potential by the DC extraction field of the TOF-MS (we plan to delay the TOF-MS fields to switch on just after ionization in the future). To find the ionization energy at zero DC field, we measured the ionization threshold while varying the extraction field amplitude. We estimated the ionization threshold term value by fitting the curves to a sigmoid. We take the mid point in the raising of the step-like function to be the ionization threshold value. The results are shown in figure 18. All curves were normalized by the fitted amplitude, and the errors were determined by the fit error. We indeed see that the ionization threshold scales as $E^{-1/2}$ [44]. The slope intersects the zero electric field line at 125666 ± 1 cm^{-1}, which is within range of the value found in [35]. We considered the mid point of the sigmoid as the transition term value, but we could have used either the top or the bottom of the sigmoid as well. The black dashed lines signify the fits of using these points instead, they intersect the zero electric field line at:

$$\text{Term Energy}_{Top/Bottom} = 125662 \pm 2/125670 \pm 4 \text{ cm}^{-1},$$

Both lines are still within range of the results of [35].

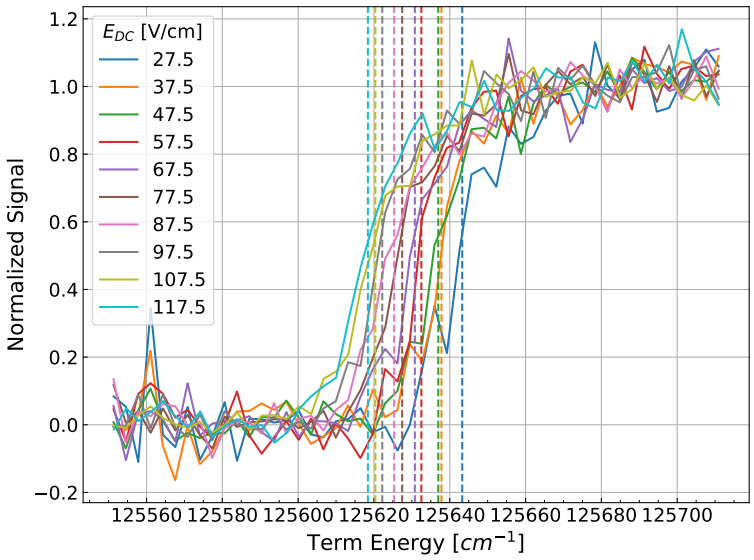

(a)

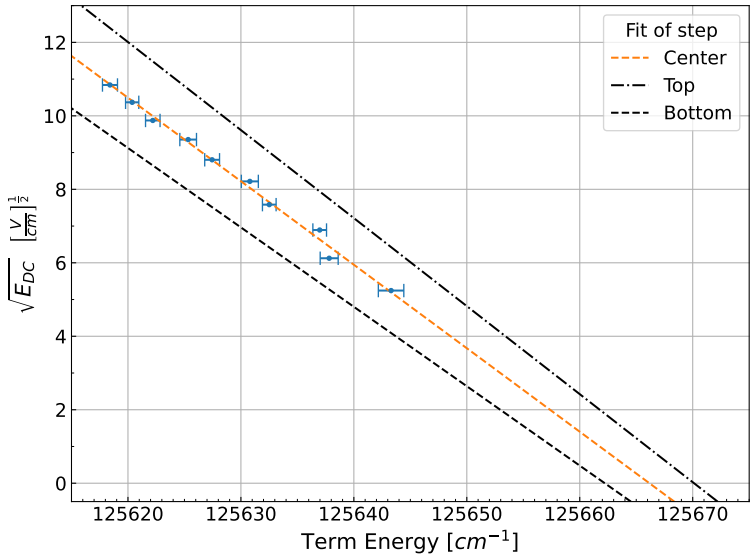

(b)

Figure 18: Ionization threshold dependence on the extraction field amplitude. (a) 2+1' REMPI scan at different extraction voltages. The dashed lines mark the position of the ionization threshold. (b) The ionization thresholds extracted from (a) with extrapolation to zero DC field at different positions of the step function, its beginning, center, and its ending.

5 Discussion

In this thesis, we built a home-made time-of-flight mass spectrometer (TOF-MS) with a molecular beam source in an ultra-high vacuum apparatus. We built and aligned the laser lines and integrated the control system hardware and software. We performed single-color and two-color ionization spectroscopy to determine the state preparation fidelity in the creation of molecular ions. All experiments were performed with N_2 of mass 28 amu, the system, however, was designed with the heavy I_2 molecule (254 amu) in mind.

As of right now, the setup still needs some minor fixes. A fast voltage switch needs to be implemented with the TOF electrodes to remove as much as possible the DC electric field shift of the ionization energy. The simulated TOF peaks arrive earlier than the actual TOF peaks (12% error), meaning that some parameters in the simulations are incorrect. These parameters still need to be identified and corrected. A scan to find the optimal voltage ratio giving the shortest TOF peaks needs to be done to validate the simulated voltage ratio and to facilitate the highest mass resolution. MS of heavier molecules needs to be done, testing the MS resolution of the setup at these mass values.

Despite the above, we now have an operable TOF-MS of a molecular beam. The MS resolution we get for N_2 is relatively high, allowing us to use it for future experiments with much heavier molecules. Using the pulsed valve, an abundance of gasses can be injected into the setup. Changing the dyes in the dye lasers can give us a wide range of wavelengths to use for REMPI. Our results are backed by the previous results of Mackenzie et al. [35, 43]. All these make this setup a dependable and flexible source for optimizing and generating molecular ions for an ion trap.

As of right now, we can generate internally cold N_2^+ by tuning our dye lasers to the S(0) transition and to the ionization threshold. The next step is to connect this setup to an ion trap and redirect the REMPI lasers into the center of the trap in order to trap the cold molecules. Another plan for the near future is to switch the REMPI wavelengths to try and use the more selective REMPI method suggested by Gardner et al. [27].

A possibly different direction can be to use the setup in order to optimize the generation of I_2^+ molecular ions. This molecule's heavy mass and unique electronic ground-state structure make it a viable candidate for searching for dark matter [26] (an ongoing collaboration with the group of Prof. Gilad Perez). Generating a sufficient pressure of I_2 gas, which is solid at room temperature, may require heating I_2 to about 100 °C. This will require changing the APV to a pulsed valve more suitable for heating. A high-temperature Even-Lavie valve [45] was purchased for this purpose. This will be a more challenging direction as not many experiments were done with I_2 REMPI, but an exciting

direction still, since ground-state cooling and quantum control of single I_2^+ molecules has never been shown.

This being the first setup in the lab, this project is a good foundation for experimenting with the quantum mechanics of molecular ions. Although there is still a long way to go, the success of this project is a stepping stone for the wonderful experiments planned ahead.

Literature

[1] Serge Haroche. "Nobel Lecture: Controlling photons in a box and exploring the quantum to classical boundary." In: *Rev. Mod. Phys.* 85 (3 July 2013), pp. 1083–1102. DOI: 10.1103/RevModPhys.85.1083. URL: https://link.aps.org/doi/10.1103/RevModPhys.85.1083.

[2] David J. Wineland. "Nobel Lecture: Superposition, entanglement, and raising Schrödinger's cat." In: *Rev. Mod. Phys.* 85 (3 July 2013), pp. 1103–1114. DOI: 10.1103/RevModPhys.85.1103. URL: https://link.aps.org/doi/10.1103/RevModPhys.85.1103.

[3] H. S. Margolis. "Optical frequency standards and clocks." In: *Contemporary Physics* 51.1 (2010), pp. 37–58. DOI: 10.1080/00107510903257616. eprint: https://doi.org/10.1080/00107510903257616. URL: https://doi.org/10.1080/00107510903257616.

[4] Jérôme Lodewyck. "On a definition of the SI second with a set of optical clock transitions." In: *Metrologia* 56.5 (Sept. 2019), p. 055009. DOI: 10.1088/1681-7575/ab3a82. URL: https://dx.doi.org/10.1088/1681-7575/ab3a82.

[5] Lincoln D Carr et al. "Cold and ultracold molecules: science, technology and applications." In: *New Journal of Physics* 11.5 (May 2009), p. 055049. DOI: 10.1088/1367-2630/11/5/055049. URL: https://dx.doi.org/10.1088/1367-2630/11/5/055049.

[6] D. Mitra, K. H. Leung, and T. Zelevinsky. "Quantum control of molecules for fundamental physics." In: *Phys. Rev. A* 105 (4 Apr. 2022), p. 040101. DOI: 10.1103/PhysRevA.105.040101. URL: https://link.aps.org/doi/10.1103/PhysRevA.105.040101.

[7] Fabian Wolf et al. "Non-destructive state detection for quantum logic spectroscopy of molecular ions." In: *Nature* 530.7591 (Feb. 2016), pp. 457–460. ISSN: 1476-4687. DOI: 10.1038/nature16513. URL: https://doi.org/10.1038/nature16513.

[8] Mudit Sinhal et al. "Quantum-nondemolition state detection and spectroscopy of single trapped molecules." In: *Science* 367.6483 (2020), pp. 1213–1218. DOI: 10.1126/science.aaz9837. eprint: https://www.science.org/doi/pdf/10.1126/science.aaz9837. URL: https://www.science.org/doi/abs/10.1126/science.aaz9837.

[9] Chin-wen Chou et al. "Preparation and coherent manipulation of pure quantum states of a single molecular ion." In: *Nature* 545.7653 (May 2017), pp. 203–207. ISSN: 1476-4687. DOI: 10.1038/nature22338. URL: https://doi.org/10.1038/nature22338.

[10] Yiheng Lin et al. “Quantum entanglement between an atom and a molecule.” In: *Nature* 581.7808 (May 2020), pp. 273–277. ISSN: 1476-4687. DOI: 10.1038/s41586-020-2257-1. URL: https://doi.org/10.1038/s41586-020-2257-1.

[11] Kaveh Najafian, Ziv Meir, and Stefan Willitsch. “From megahertz to terahertz qubits encoded in molecular ions: theoretical analysis of dipole-forbidden spectroscopic transitions in N2+.” In: *Phys. Chem. Chem. Phys.* 22 (40 2020), pp. 23083–23098. DOI: 10.1039/D0CP03906C. URL: http://dx.doi.org/10.1039/D0CP03906C.

[12] Sayan Patra et al. “Proton-electron mass ratio from laser spectroscopy of HD+ at the part-per-trillion level.” In: *Science* 369.6508 (2020), pp. 1238–1241. DOI: 10.1126/science.aba0453. eprint: https://www.science.org/doi/pdf/10.1126/science.aba0453. URL: https://www.science.org/doi/abs/10.1126/science.aba0453.

[13] S. Alighanbari et al. “Precise test of quantum electrodynamics and determination of fundamental constants with HD+ ions.” In: *Nature* 581.7807 (May 2020), pp. 152–158. ISSN: 1476-4687. DOI: 10.1038/s41586-020-2261-5. URL: https://doi.org/10.1038/s41586-020-2261-5.

[14] Wolfgang Paul. “Electromagnetic traps for charged and neutral particles.” In: *Rev. Mod. Phys.* 62 (3 July 1990), pp. 531–540. DOI: 10.1103/RevModPhys.62.531. URL: https://link.aps.org/doi/10.1103/RevModPhys.62.531.

[15] Colin D. Bruzewicz et al. “Trapped-ion quantum computing: Progress and challenges.” In: *Applied Physics Reviews* 6.2 (2019), p. 021314. DOI: 10.1063/1.5088164. eprint: https://doi.org/10.1063/1.5088164. URL: https://doi.org/10.1063/1.5088164.

[16] F. Diedrich et al. “Laser Cooling to the Zero-Point Energy of Motion.” In: *Phys. Rev. Lett.* 62 (4 Jan. 1989), pp. 403–406. DOI: 10.1103/PhysRevLett.62.403. URL: https://link.aps.org/doi/10.1103/PhysRevLett.62.403.

[17] K. Mølhave and M. Drewsen. “Formation of translationally cold MgH^+ and MgD^+ molecules in an ion trap.” In: *Phys. Rev. A* 62 (1 June 2000), p. 011401. DOI: 10.1103/PhysRevA.62.011401. URL: https://link.aps.org/doi/10.1103/PhysRevA.62.011401.

[18] P. O. Schmidt et al. “Spectroscopy Using Quantum Logic.” In: *Science* 309.5735 (2005), pp. 749–752. DOI: 10.1126/science.1114375. eprint: https://www.science.org/doi/pdf/10.1126/science.1114375. URL: https://www.science.org/doi/abs/10.1126/science.1114375.

[19] D Leibfried. “Quantum state preparation and control of single molecular ions.” In: *New Journal of Physics* 14.2 (Feb. 2012), p. 023029. DOI: 10.1088/1367-2630/14/2/023029. URL: https://dx.doi.org/10.1088/1367-2630/14/2/023029.

[20] S Ding and D N Matsukevich. “Quantum logic for the control and manipulation of molecular ions using a frequency comb.” In: *New Journal of Physics* 14.2 (Feb. 2012), p. 023028. DOI: 10.1088/1367-2630/14/2/023028. URL: https://dx.doi.org/10.1088/1367-2630/14/2/023028.

[21] J. Martin Berglund, Michael Drewsen, and Christiane P. Koch. “Fundamental bounds on rotational state change in sympathetic cooling of molecular ions.” 2019. DOI: 10.48550/ARXIV.1905.02130. URL: https://arxiv.org/abs/1905.02130.

[22] Xin Tong, Alexander H Winney, and Stefan Willitsch. “Sympathetic cooling of molecular ions in selected rotational and vibrational states produced by threshold photoionization.” In: *Physical review letters* 105.14 (2010), p. 143001.

[23] A. K. Hansen et al. “Efficient rotational cooling of Coulomb-crystallized molecular ions by a helium buffer gas.” In: *Nature* 508.7494 (Apr. 2014), pp. 76–79. ISSN: 1476-4687. DOI: 10.1038/nature12996. URL: https://doi.org/10.1038/nature12996.

[24] *Ion trapping groups worldwide*. https://quantumoptics.at/en/links/ion-trapping-worldwide.html. Accessed: 2023-01-23.

[25] Masatoshi Kajita et al. “Test of m_p/m_e changes using vibrational transitions in N_2^+.” In: *Phys. Rev. A* 89 (3 Mar. 2014), p. 032509. DOI: 10.1103/PhysRevA.89.032509. URL: https://link.aps.org/doi/10.1103/PhysRevA.89.032509.

[26] L. F. Pa šteka et al. “Search for the variation of fundamental constants: Strong enhancements in $X\ ^2\square$ cations of dihalogens and hydrogen halides.” In: *Phys. Rev. A* 92 (1 July 2015), p. 012103. DOI: 10.1103/PhysRevA.92.012103. URL: https://link.aps.org/doi/10.1103/PhysRevA.92.012103.

[27] Amy Gardner, Timothy Softley, and Matthias Keller. “Multi-photon ionisation spectroscopy for rotational state preparation of N2+.” In: *Scientific Reports* 9.1 (Jan. 2019), p. 506. ISSN: 2045-2322. DOI: 10.1038/s41598-018-36783-5. URL: https://doi.org/10.1038/s41598-018-36783-5.

[28] Stefan Willitsch. "Coulomb-crystallised molecular ions in traps: methods, applications, prospects." In: *International Reviews in Physical Chemistry* 31.2 (2012), pp. 175–199. DOI: 10.1080/0144235X.2012.667221. eprint: https://doi.org/10.1080/0144235X.2012.667221. URL: https://doi.org/10.1080/0144235X.2012.667221.

[29] Michael D. Morse. "2 - Supersonic Beam Sources." In: *Atomic, Molecular, and Optical Physics: Atoms and Molecules*. Ed. by F.B. Dunning and Randall G. Hulet. Vol. 29. Experimental Methods in the Physical Sciences. Academic Press, 1996, pp. 21–47. DOI: https://doi.org/10.1016/S0076-695X(08)60784-X. URL: https://www.sciencedirect.com/science/article/pii/S0076695X0860784X.

[30] K. Luria, W. Christen, and U. Even. "Generation and Propagation of Intense Supersonic Beams." In: *The Journal of Physical Chemistry A* 115.25 (2011). PMID: 21486054, pp. 7362–7367. DOI: 10.1021/jp201342u. eprint: https://doi.org/10.1021/jp201342u. URL: https://doi.org/10.1021/jp201342u.

[31] Nicholas R. Hutzler, Hsin-I Lu, and John M. Doyle. "The Buffer Gas Beam: An Intense, Cold, and Slow Source for Atoms and Molecules." In: *Chemical Reviews* 112.9 (2012). PMID: 22571401, pp. 4803–4827. DOI: 10.1021/cr200362u. eprint: https://doi.org/10.1021/cr200362u. URL: https://doi.org/10.1021/cr200362u.

[32] Dudley Herschbach. "Atomic and Molecular Beams in Chemical Physics: A Continuing Odyssey." In: *Atomic and Molecular Beams: The State of the Art 2000*. Ed. by Roger Campargue. Berlin, Heidelberg: Springer Berlin Heidelberg, 2001, pp. 3–40. ISBN: 978-3-642-56800-8. DOI: 10.1007/978-3-642-56800-8_1. URL: https://doi.org/10.1007/978-3-642-56800-8_1.

[33] U. Even. "Pulsed Supersonic Beams from High Pressure Source: Simulation Results and Experimental Measurements." In: *Advances in Chemistry* 2014 (Aug. 2014), p. 636042. ISSN: 2356-6612. DOI: 10.1155/2014/636042. URL: https://doi.org/10.1155/2014/636042.

[34] Ulrich Boesl and Ralf Zimmermann. "Fundamentals and Mechanisms of Resonance-Enhanced Multiphoton Ionization (REMPI) in Vacuum and its Application in Molecular Spectroscopy." In: *Photoionization and Photo Induced Processes in Mass Spectrometry*. John Wiley & Sons, Ltd, 2021. Chap. 2, pp. 23–88. ISBN: 9783527682201. DOI: https://doi.org/10.1002/9783527682201.ch2. eprint: https://onlinelibrary.wiley.com/doi/pdf/10.1002/

9783527682201.ch2. URL: https://onlinelibrary.wiley.com/doi/abs/10.1002/9783527682201.ch2.

[35] S.R. Mackenzie et al. "Rotational state selectivity in N2 + X 2∑g +(v+ = 0) by delayed pulsed field ionization spectroscopy via the a″ 1∑g + (v′ = 0) state." In: *Molecular Physics* 86.5 (1995), pp. 1283–1297. DOI: 10.1080/00268979500102731. eprint: https://doi.org/10.1080/00268979500102731. URL: https://doi.org/10.1080/00268979500102731.

[36] Michael Guilhaus. "Special feature: Tutorial. Principles and instrumentation in time-of-flight mass spectrometry. Physical and instrumental concepts." In: *Journal of Mass Spectrometry* 30.11 (1995), pp. 1519–1532. DOI: https://doi.org/10.1002/jms.1190301102. eprint: https://analyticalsciencejournals.onlinelibrary.wiley.com/doi/pdf/10.1002/jms.1190301102. URL: https://analyticalsciencejournals.onlinelibrary.wiley.com/doi/abs/10.1002/jms.1190301102.

[37] M. M. Wolff and W. E. Stephens. "A Pulsed Mass Spectrometer with Time Dispersion." In: *Review of Scientific Instruments* 24.8 (1953), pp. 616–617. DOI: 10.1063/1.1770801. eprint: https://doi.org/10.1063/1.1770801. URL: https://doi.org/10.1063/1.1770801.

[38] W. C. Wiley and I. H. McLaren. "Time-of-Flight Mass Spectrometer with Improved Resolution." In: *Review of Scientific Instruments* 26.12 (1955), pp. 1150–1157. DOI: 10.1063/1.1715212. eprint: https://doi.org/10.1063/1.1715212. URL: https://doi.org/10.1063/1.1715212.

[39] Ulrich Boesl. "Time-of-flight mass spectrometry: Introduction to the basics." In: *Mass Spectrometry Reviews* 36.1 (2017), pp. 86–109. DOI: https://doi.org/10.1002/mas.21520. eprint: https://analyticalsciencejournals.onlinelibrary.wiley.com/doi/pdf/10.1002/mas.21520. URL: https://analyticalsciencejournals.onlinelibrary.wiley.com/doi/abs/10.1002/mas.21520.

[40] *Grafana*. https://grafana.com/grafana/. Accessed: 2023-01-23.

[41] D Manura and D Dahl. *SIMION (R) 8.0 User Manual, Scientific Instrument Services, Inc., Ringoes, NJ 08551 (2008)*.

[42] *Quantum Machines OPX+*. https://www.quantum-machines.co/opx+/. Quote from: https://qm-docs.qualang.io/introduction/qop_overview.

[43] F. Merkt, S. R. Mackenzie, and T. P. Softley. “Rotational autoionization dynamics in high Rydberg states of nitrogen.” In: *The Journal of Chemical Physics* 103.11 (1995), pp. 4509–4518. DOI: 10.1063/1.470639. eprint: https://doi.org/10.1063/1.470639. URL: https://doi.org/10.1063/1.470639.

[44] William A. Chupka. “Factors affecting lifetimes and resolution of Rydberg states observed in zero electron kinetic□energy spectroscopy.” In: *The Journal of Chemical Physics* 98.6 (1993), pp. 4520–4530. DOI: 10.1063/1.465011. eprint: https://doi.org/10.1063/1.465011. URL: https://doi.org/10.1063/1.465011.

[45] *Even-Lavie Valves*. https://sites.google.com/site/evenlavievalve/available-types. Accessed: 2023-02-11.